

New estimates of leaf angle distribution from terrestrial LiDAR: Comparison with measured and modelled estimates from nine broadleaf tree species

Matheus Boni Vicari^{a,*}, Jan Pisek^{b,1}, Mathias Disney^{a,c}

^a Department of Geography, University College London, Pearson Building, Gower Street, London, WC1E 6BT, London, UK

^b Tartu Observatory, University of Tartu, Observatooriumi 1, Tõravere, 61602, Tartumaa, Estonia

^c NERC National Centre for Earth Observation (NCEO), UK

ARTICLE INFO

Keywords:

Leaf angle distribution (LAD)
Terrestrial LiDAR scanning (TLS)
Digital photography
3D
Monte Carlo ray tracing (MCRT)
Radiative transfer

ABSTRACT

Leaf angle distribution (LAD) is an important property which influences the spectral reflectance and radiation transmission properties of vegetation canopies, and hence interception, absorption and photosynthesis. It is a fundamental parameter of radiative transfer models of vegetation at all scales. Yet, the difficulty in measuring LAD causes it to be also one of the most poorly characterized parameters, and is typically either assumed to be random, or to follow one of a very small number of parametric ‘archetype’ functions. Terrestrial LiDAR scanning (TLS) is increasingly being used to measure canopy structure, but LAD estimation from TLS has been limited thus far. We introduce a fast and simple method for detection of LAD information from terrestrial LiDAR scanning (TLS) point clouds. Here, it is shown that LAD information can be obtained by simply accumulating all valid planes fitted to points in a leaf point cloud. As points alone do not have any normal vector, subsets of points around each point are used to calculate the normal vectors. Importantly, for the first time we demonstrate the effect of distance on the reliable LAD information retrieval with TLS data. We test, validate, and compare the TLS-based method with established leveled digital photography (LDP) approach. We do this using data from both real trees covering the full range of existing leaf angle distribution type, but also from 3D Monte Carlo ray tracing. Crucially, this latter approach allows us to simulate both images and TLS point clouds from the same trees, for which the LAD is known explicitly a priori. This avoids the difficulty of assessing LAD manually, which being a difficult and potentially error-prone process, is an additional source of error in assessing the accuracy of LAD extraction methods from TLS or photography. We show that compared to the LDP measurement technique, TLS is not limited by leaf curvature, and depending on the distance of the TLS from the target, is potentially capable of retrieving leaf angle information from more complex, non-flat leaf surfaces. We demonstrate the possible limitation of TLS measurement techniques for the retrieval of LAD information for more distant canopies, or for taller trees ($h > 20$ m).

1. Introduction

The leaf angle distribution (LAD) is a key property of vegetation canopies, and is therefore vital for models used to represent and understand the plant canopy processes of photosynthesis, evapotranspiration, radiative transfer (RT), and hence spectral reflectance and absorptance (Warren Wilson, 1959; Lemeur and Blad, 1974; Ross, 1981; Myneni et al., 1989; Asner, 1998; Stuckens et al., 2009). Yet, despite the strong sensitivity of many of these models to variability in LAD, the difficulty in measuring LAD often causes it to be one of the most poorly constrained parameters in structural models of canopy radiative transfer (see e.g. Ollinger, 2011). As a result, LAD is very often

assumed to be random, or spherical in order to simplify the process of modelling RT in vegetation, without clear justification or quantified impact of the resulting uncertainty. Improving methods for measuring LAD is thus essential for advancing ecological understanding of its role within the biophysical interaction of sunlight and the forest canopy, and how we can better represent it within canopy models.

Various methods and instruments have been proposed over the years for in situ measurement of leaf inclination angles (e.g., Lang, 1973; Smith and Berry, 1979; Kucharik et al., 1998; Falster and Westoby, 2003; Hosoi and Omasa, 2007; Müller-Linow et al., 2015). However, their wide-spread use has been generally hampered by difficulties in applying them to tall (and closed) canopies, their

* Corresponding author.

E-mail address: matheus.vicari.15@ucl.ac.uk (M.B. Vicari).

¹ Joint first authorship.

unsatisfactory ability to reproduce measurements, or high costs.

Ryu et al. (2010) proposed a robust, simple method to identify leaf angles from leveled digital photography (LDP) and to provide reliable LAD information for broadleaf trees. The LDP method was also found to be comparable to manual clinometer measurements (Pisek et al., 2011). McNeil et al. (2016) implemented the LDP method successfully on images collected with digital cameras mounted onboard unmanned aerial vehicles (UAV). While this method has been shown to be more efficient compared to the earlier approaches mentioned above (Zou et al., 2014), the need for manual, non-automated identification of suitable leaves for LAD determination, and the regulatory and piloting challenges with UAVs still pose drawbacks that hinder more effective and widespread use of the LDP method.

With mm-level ranging accuracy and fine resolution allowing the capture of very detailed 3-D structural information of a canopy, terrestrial LiDAR scanning (TLS) technology might be able to overcome the shortcomings of the conventional means of measuring LAD profile of the canopy. So far, TLS has been shown to be able to provide more detailed information about tree properties such as diameter at breast height (DBH) (Bauwens et al., 2016), height (Király and Broly, 2007; Prasad et al., 2016; Palace et al., 2016), aboveground biomass (Calders et al., 2013, 2015; Tanago et al., 2018; Disney et al., 2018) and overall structure (Côté et al., 2012; Raunonen et al., 2013; Hackenberg et al., 2014a,b; Malhi et al., 2018). There have been already several attempts to measure leaf orientation with TLS data. Jin et al. (2015) estimated leaf angles from averaging normal vectors of clustered leaves and obtained a correlation coefficient of 0.96 for a validation using a single camphorwood tree. Zheng and Moskal (2012) also proposed the use of normal vectors to estimate leaf angle but calculated from subsets of points. This latter method was able to predict leaf inclination with R squares of 0.73 and 0.573 for big leaf maple tree and sugar maple, respectively. Bailey and Mahaffee (2017) is another example of approach using normal vectors but estimated for triangulated surfaces from the point cloud. Zhao et al. (2015) presented a physical-statistical approach using Maximum Likelihood Estimates to infer leaf properties from TLS data. Although all these methods showed potential, their increased algorithm complexity and possible uncertainties must be noted: dependency of clustering or triangulation algorithms in preliminary steps (Jin et al., 2015; Bailey and Mahaffee, 2017); dependency of model and parameters selection (Zhao et al., 2015); or presence of noisy data (Bailey and Mahaffee, 2017). Also, only a very limited set of trees, usually of small size, and simple simulations were used for validation of these methods. Effects caused by larger laser footprint, i.e. larger trees (> 40 m) or longer scanning distances, have also not been tested and have the potential to limit accuracy.

In this work, we introduce a method that is based on simple assumptions and fast (i.e. processing times under 2 min per tree on a consumer-grade processor) for detection of LAD information from TLS point clouds. Importantly, for the first time we demonstrate the effect of TLS distance on the retrieval of accurate LAD information from TLS data. We test, validate, and compare the TLS-based method with the LDP approach by Ryu et al. (2010) using real trees covering the full range existing leaf angle distribution types. Crucially, we also address one of the key issues that can hinder validating LAD measurement: the difficulty of obtaining accurate known LAD information to compare with values derived from LDP, TLS etc. Here, we augment the comparison of methods using real trees, by using very detailed 3D model trees to simulate LDP and TLS measurements, but with LAD known a priori. This allows us to compare LAD estimates against 'true' values without having to worry about the uncertainty of the true values.

2. Materials and methods

2.1. Study sites and tree species

We measured leaf inclination angles on four broadleaf tree species

from the Royal Botanic Gardens, Kew, the United Kingdom (51.478 °N, 0.295 °W). We also used model representations of another five tree species used to reconstruct actual canopy of the Järvselja birch stand in Estonia (58.277 °N; 27.341 °E) (Kuusk et al., 2013) in the fourth phase of RAdiative transfer Model Intercomparison (RAMI-IV) exercise (Widłowski et al., 2015).

The leaf inclination angle measurements from the Royal Botanic Gardens at Kew were made on individual trees with separate tree crowns on 17 October 2017. The sampled tree species included Japanese hop hornbeam (*Ostrya japonica*), date plum (*Diospyros lotus*), maidenhair tree (*Ginkgo biloba*), and Wollemi pine (*Wollemia nobilis*).

2.2. Terrestrial laser scanner data: simulated and measured

2.2.1. Simulated terrestrial laser scanner point clouds

Synthetic TLS clouds were generated for five 3D scenes, which are comprised of a single tree model in the origin of an infinite plane. These stands have been generated as part of the 4th phase of the Radiative Transfer Model Intercomparison (RAMI) exercise², to provide realistic scenes for canopy model benchmarking (Widłowski et al., 2015). Here, we used the RAMI-IV representations of the Järvselja birch stand (summer)³. The full RAMI 1 ha scene contains 1029 trees, comprising 18 individual variant trees of 7 species: Norway maple (*Acer platanoides*; ACPL), common alder (*Alnus glutinosa*; RAMI-IV representation code ALGL3), Silver birch (*Betula pendula*; BEPE2), common ash (*Fraxinus excelsior*; FREX), and small-leaved lime (*Tilia cordata*; TICO2). Here, we use a subset of 5 of these trees to simulate TLS point clouds, using the librat, Monte-Carlo ray tracing (MCRT) library (Fig. 1) (Lewis, 1999; Disney et al., 2006, 2011). The librat model is one of two models that provide the 'most credible' full 3D RT model solutions in the RAMI exercise and form the basis of the RAMI Online Model Checker (ROMC), a community tool for benchmarking more approximate RT models (Widłowski et al., 2008). Librat has been used to simulate canopy properties and LiDAR point clouds for a number of applications (Disney et al., 2009, 2010; Hackenberg et al., 2014a,b; Woodgate et al., 2016). The leaves of each of the RAMI-IV trees are oriented explicitly for each tree, and so their individual angles are known exactly a priori.

Librat TLS simulations were performed at 120 different locations around each tree, set in a regular grid with 10 m spacing (Fig. 2). As each simulated cloud has material information, only leaf points were kept in further steps for LAD estimates. The simulated scan angle resolution was 0.04°, resulting in a point cloud with point density and resolution similar to the measured point cloud. In order to avoid introducing uncertainties from partial returns, beam divergence was infinitely small. Although this is not realistic, the fact that our field data is also filtered to reduce the number of points that resulted from partial hits makes this assumption less relevant in the validation of our method. For each tree, we used combinations of 4 point clouds, located 90° apart at the same 10 m interval (Fig. 2 and Fig. 3A).

2.2.2. Measured TLS data

Real tree LiDAR data was obtained at Kew using a Riegl VZ-400 laser scanner (RIEGL Laser Measurement Systems GmbH, Horn, Austria). This scanner has a range close to 700 m, wavelength of 1550 nm, beam divergence of 0.35 mrad and in the case of this study an angular resolution of 0.04° was used. The scanner was supported by a tripod at 1.5 m above the ground and placed in 4 different locations, approximately 90° apart and around 5 m from each tree. A set of 5 cylindrical reflectors supported by garden poles were placed around each tree to assist in co-registration of the 4 separate point clouds.

² <http://rami-benchmark.jrc.ec.europa.eu/HTML/>

³ http://rami-benchmark.jrc.ec.europa.eu/HTML/RAMI-IV/EXPERIMENTS4/ACTUAL_CANOPIES/JARVSELJA_SUMMER_BIRCHSTAND/JARVSELJA_SUMMER_BIRCHSTAND.php/.



Fig. 1. Example of simulated RAMI IV tree representations; A – *Acer platanoides* (ACPL); B – *Betula pendula* (BEPE2).

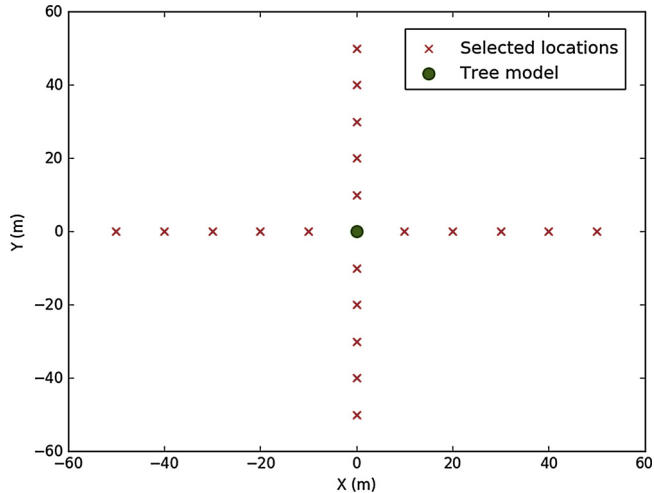


Fig. 2. Locations of simulated scans selected to validate our TLS method.

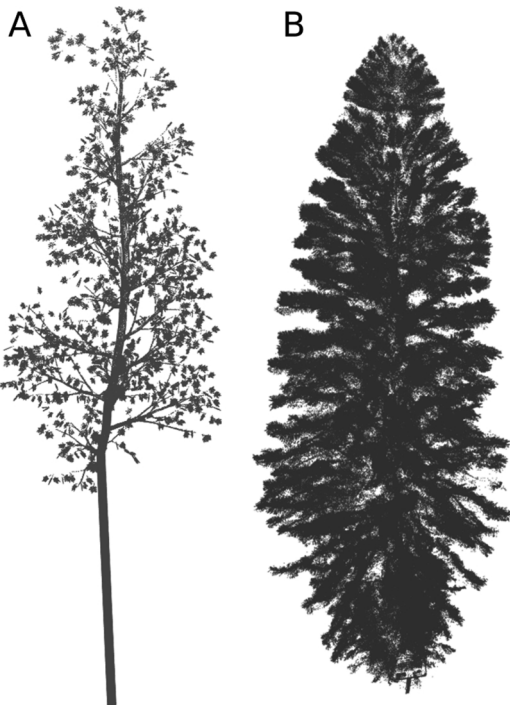


Fig. 3. Examples of simulated point cloud, Norway maple (*Acer platanoides*; ACPL) - A; and scanned point cloud, Wollemi pine (*Wollemia nobilis*) - B.

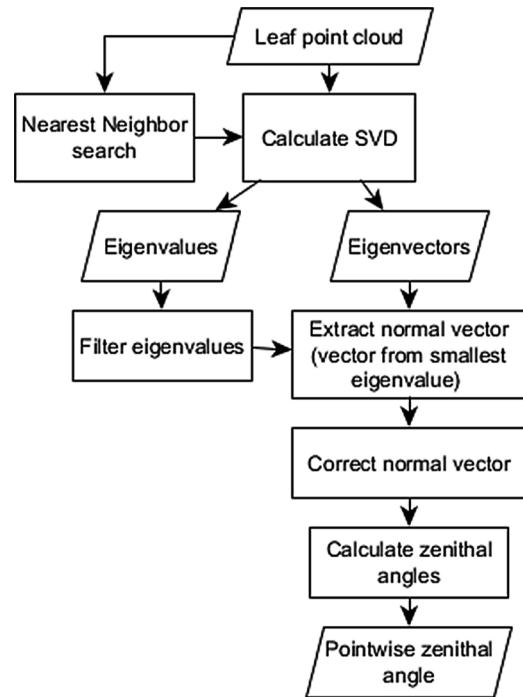


Fig. 4. LAD retrieval algorithm from TLS data. SVD refers to Singular Value Decomposition.

Scans were co-registered and filtered by pulse shape deviation to remove “noisy” data, i.e. partial laser hits (Pfennigbauer and Ullrich, 2010) using RiSCAN Pro (RIEGL Laser Measurement Systems GmbH, Horn, Austria). Trees were manually extracted from registered point clouds in CloudCompare (CloudCompare) (Fig. 3B). Materials were separated using TLSeparation Python package (Vicari, 2017) and only leaf points were kept.

2.2.3. Leaf inclination angle retrieval from TLS data

Our algorithm (Fig. 4) assumes that LAD can be obtained by simply accumulating all valid planes fitted to points in a leaf point cloud. As points alone do not have any normal vector, subsets of points around each point are used to calculate the normal vectors. The LAD algorithm starts by performing a Nearest Neighbors search around each point in the leaf cloud, using a fixed number of neighbors (kNN) for each point neighborhood. kNN values were tested in a sensitivity analysis (Section 2.2.4) and a value of 10 points was selected for our point clouds. The value of this parameter should be a compromise between a neighborhood of points small enough as to reduce the occurrence of angles calculated from more than a single leaf, but still with a number of points sufficient to minimize the impact of noise in the data. We opted for a fixed kNN value in our method in order to speed up processing while also being robust (see Section 2.2.4.). Even though a fixed kNN setting might generate neighborhoods of variable size, pre-processing steps and the further filtering of neighborhoods (see below) help to mitigate negative impacts which this parameter might cause on angle estimates.

Next, Singular Value Decomposition (SVD) is used to perform a surface regression analysis (plane fitting) on each subset of points (Fig. 5). Through SVD a set of eigenvalues and eigenvectors is calculated for each point. Eigenvectors relative to the smallest of 3 eigenvalues, in a 3D space, are equivalent to the normal vector of the fitted plane (Mandel, 1982; Klasing, 2009). As normal vectors calculated using SVD are susceptible to outliers, a filtering step ensures that only normal vectors from points that are close enough to a plane are kept. The smallest eigenvalue, in a 3D space, is a direct expression of how close to a plane the set of points is. To standardize all eigenvalues into a

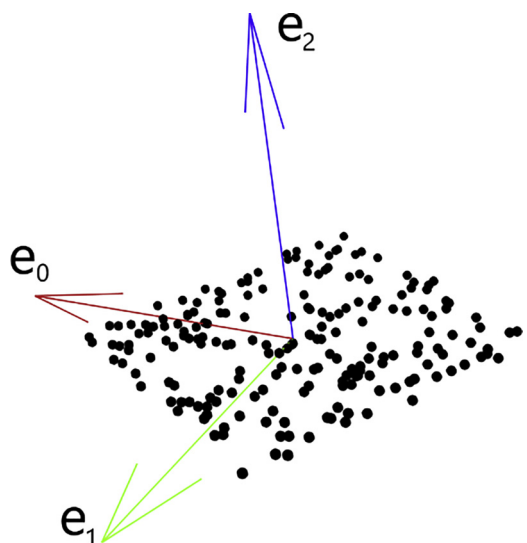


Fig. 5. Example of a set of eigenvectors calculated for a random set of points that represent a plane. Sub-indices of e represent eigenvectors relative to eigenvalues from largest (0) to smallest (2). In this example, e_2 represents the normal vector of a plane fitted to all points shown.

common range (0 to 1), the eigenvalue ratios were calculated for each point, dividing each eigenvalue by the sum of all three eigenvalues. The sensitivity analysis was also used to select this parameter's value and, therefore, only points with the third eigenvalue ratio lower than 0.1, were kept (Fig. 6). This filtering step ensures that points in intersecting regions or with strong presence of noise are not used in the LAD estimation.

Filtered vectors (N^-) pointing downwards, i.e. negative z-axis component, were inverted by multiplying them by -1:

$$N^+ = \begin{cases} N^-_z \geq 0, N^- \\ N^-_z < 0, N^* - 1 \end{cases} \quad (1)$$

The inclination angle, in degrees, for each point (α_i) is obtained by calculating the angle between corrected normal vectors (N^+_i) and a zenith vector (z^-) defined as (0, 0, 1). A final multiplication by (180 / pi) is used to convert the final value to degrees:

$$\alpha_i = \cos^{-1} \left(\frac{z^- \cdot N^+_i}{\|z^-\| \cdot \|N^+_i\|} \right) * \left(\frac{180}{\pi} \right) \quad (2)$$

The algorithm produces one inclination angle value for each valid plane in the leaf point cloud (Fig. 7). This means that every leaf will produce multiple inclination angles, one for each valid plane patch. To

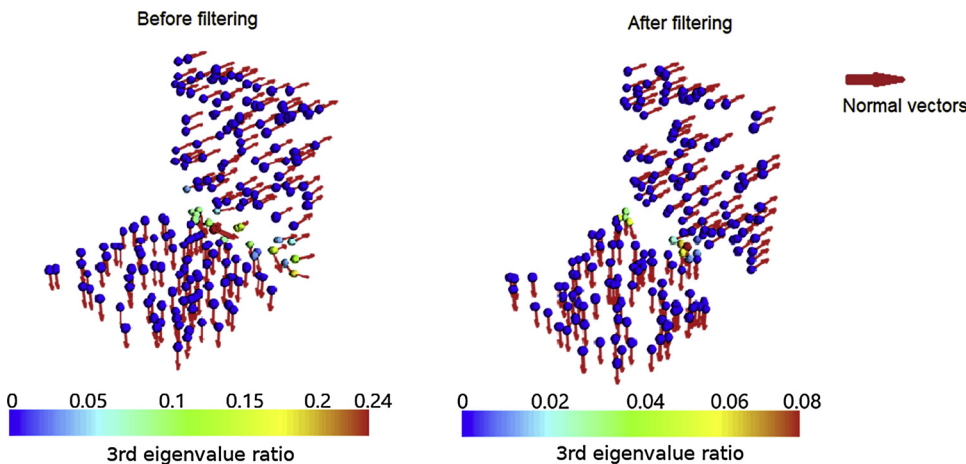


Fig. 6. Example of normal vectors filtering by eigenvalue ratio threshold. Vectors relative to points with third eigenvalue ratio higher than 0.1 were removed. To define local neighborhoods and calculate the eigenvalues, 10 points around each point shown in this figure were selected (knn = 10) (For interpretation of the references to colour in this figure legend, the reader is referred to the web version of this article).

generate the final LAD, point-wise angles are aggregated (Fig. 8D).

In order to better understand how robust our TLS method is, given different input parameters, we performed a sensitivity analysis using the simulated point clouds. Also, as an example of possible application of our TLS method, Fig. 8E shows azimuth angles for different height slices along the tree height.

2.2.4. Sensitivity analysis of LAD estimates from simulated data

The sensitivity analysis was performed using the same simulated point clouds as in the LAD comparison. A set of values for knn (5, 10, 15, 20, 25, 50, 100) and eigenvalue ratio threshold (0.05, 0.1, 0.15, 0.2, 0.25, 0.3, 0.5) were combined iteratively and used to process every tree point cloud, from different scanning distances, generating 1225 estimates in total. Resulting distributions were binned in intervals of 5° and compared against their respective reference LAD using Mean Absolute Error (MAE).

We also investigated the impact of scanning distance in the TLS LAD estimates by calculating the difference between each tree's LAD for scanning distances of 10 and 50 m. The difference was calculated, using MAE, for all simulated point clouds, except those from tree model FREX. Point clouds from this tree were not considered in the distance analysis because its leaves model employs 11 leaves with different area, and so, could not be assessed in the same way as for the other trees.

A validation test was also developed to evaluate the TLS LAD accuracy for different leaf curvatures. We used the single leaves from the same leaf models from the four RAMI-IV trees used in our simulated dataset. A set point clouds were simulated for each leaf, varying point density and leaf curvature, and also varying knn values used to estimate the leaf angles. Pointwise angles were estimated for each leaf point cloud and aggregated into LADs. Each LAD was quantitatively compared (MAE) to the expected LAD from its respective simulated curved leaf. In the case of this validation leaf curvature was defined in terms of the fraction of leaf area that covers a sphere with known radius. For a flat leaf, the radius is infinite and so the curvature is assumed as 0%. A completely curved leaf, i.e. 100%, covers a sphere in a way that its extremities are touching each other.

2.3. Simulated digital photography images

Simulated LDP images of the RAMI-IV trees were also generated using the librat MCRT model (Fig. 1). Images were simulated at an equivalent resolution of 1 MP i.e. image size of 1024 × 1024 from a distance of 1.5 m from the trees in each case. Images were simulated from 4 locations around each tree for every 1 m of live crown, and with 1 ray per pixel. This means that total number of images varied from 24 (TICO2) to 48 (ALGL3). Librat image simulations have been used for various modelling applications, particularly for comparison with other

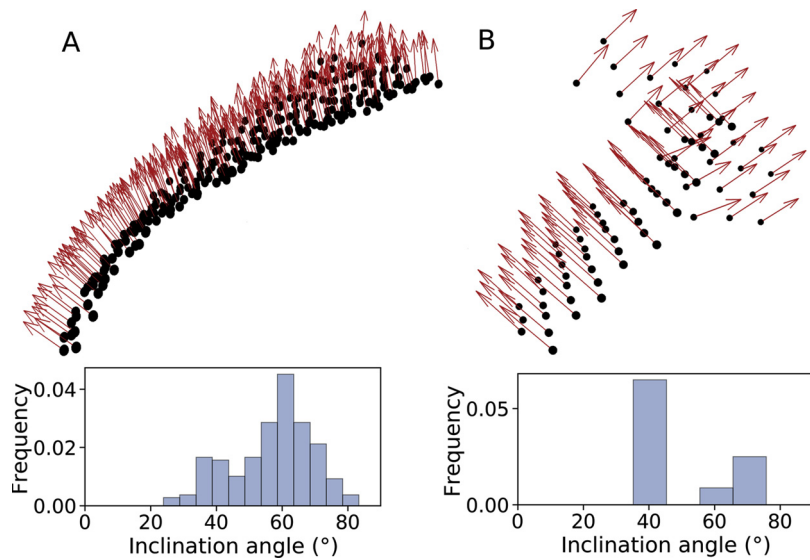


Fig. 7. Normal vectors calculated for a single leaf from field scanned *Diospyros lotus* point cloud (A) and from two neighboring leaves from TICO2 simulated point cloud (B). Respective leaf angle distributions calculated from point-wise angle are shown under each respective set of points.

canopy measurement properties such as DHP estimates of gap fraction and LAI as well as with field-measured properties (Disney et al., 2011; Woodgate et al., 2016; Origo et al., 2017).

2.4. Leveled digital photography (LDP) measurements

We used a leveled digital camera approach (Ryu et al., 2010) to measure leaf inclination angles and validate the results obtained with TLS data (Section 2.2.3). Beside the simulated images for RAMI-IV tree representations described in Section 2.2.1, we took a series of leveled digital images of tree crowns for four tree species at Kew during calm conditions (to prevent wind effects on leaves; Tadriss et al., 2014) along their full vertical tree profile. We compared two approaches to obtain

leveled digital photography: a Nikon CoolPix 4500 digital camera (4 MP) leveled and tripod-mounted, and images taken by a hand-balanced (i.e. determined by observer's feeling) Sony Xperia Z5 Compact phone equipped with 23 MP 1/2.3-inch multi-aspect BSI CMOS sensor, paired with an F2.0 lens. None of the lenses were evaluated for distortions.

Next, both simulated images of the RAMI-IV tree representations and photos obtained at Kew were visually inspected for the presence of leaves with their surfaces oriented approximately perpendicular to the viewing direction of the digital camera (Fig. 9). Inclination angles of suitable leaves were measured using the public domain image processing software ImageJ (<http://imagej.nih.gov/ij/>). It has been suggested that hundreds of leaves should be measured to obtain an accurate

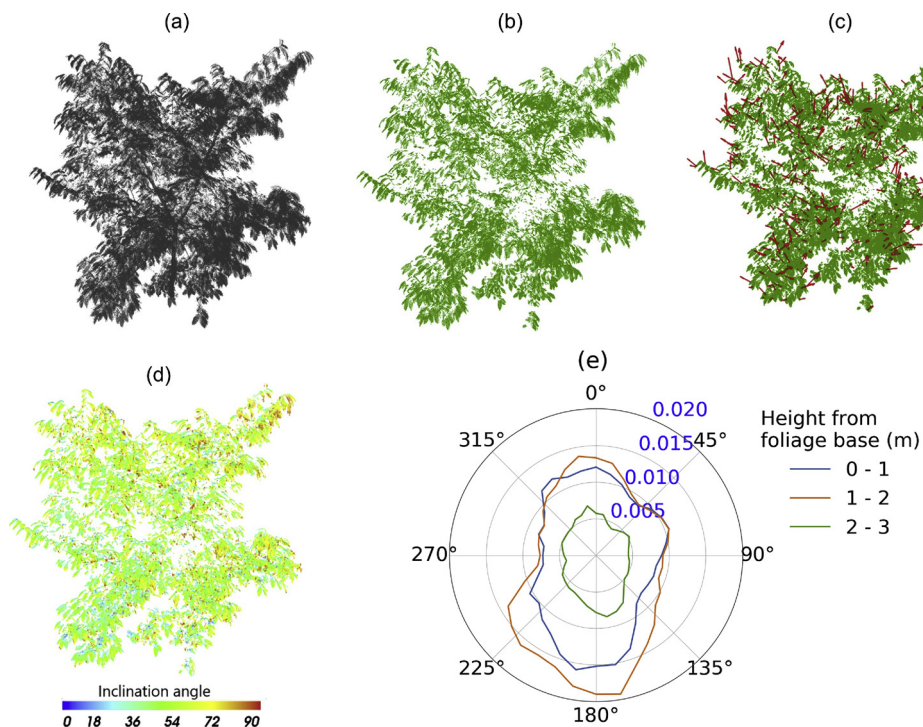


Fig. 8. *Diospyros lotus* TLS data and results. (a) Extracted point cloud. (b) Separated leaf points. (c) Examples of normal vectors (1000 vectors randomly sampled for visualization purposes only, out of around 350 thousand). (d) Pointwise leaf angle. (e) Azimuth leaf angle distribution over height slices.

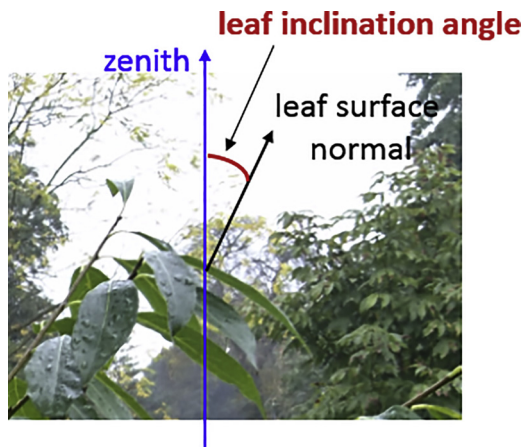


Fig. 9. A schematic diagram of the protocol used to measure leaf inclination angle from leveled digital photography (illustrated on *Diospyros lotus*).

representation of the leaf inclination angles (Kucharik et al., 1998). However, a more recent study suggests that around 75 leaves may be sufficient to obtain a representative leaf inclination angle distribution at single crown (Pisek et al., 2013). In the current work, approximately 100 leaves were measured whenever possible. Tables 1 and 2 provide the exact number of leaves collected for each species in this study.

2.5. Leaf inclination angle distribution and G-function

We estimated leaf inclination angle distribution assuming a uniform distribution of leaf azimuth angle and leaf inclination angle being independent of leaf size. The measured leaf inclination angles were fitted with the two-parameter Beta distribution (Goel and Strebel, 1984), which was shown to be the best suited for describing the probability density of θ_L (by Wang et al., 2007):

$$f(t) = \frac{1}{B(\mu, \nu)}(1 - t)^{\mu-1}t^{\nu-1} \tag{3}$$

where $t = 2\theta_L/\pi$. The Beta-distribution function $B(\mu, \nu)$ is defined as:

$$B(\mu, \nu) = \int_0^1 (1 - x)^{\mu-1}x^{\nu-1}dx = \frac{\Gamma(\mu)\Gamma(\nu)}{\Gamma(\mu + \nu)} \tag{4}$$

where Γ is the Gamma function and μ and ν are two parameters calculated as:

$$\mu = (1 - \bar{t})\left(\frac{\sigma_0^2}{\sigma_t^2} - 1\right) \tag{5}$$

$$\nu = \bar{t}\left(\frac{\sigma_0^2}{\sigma_t^2} - 1\right) \tag{6}$$

where σ_0^2 is the maximum standard deviation with expected mean \bar{t} ($\sigma_0^2 = \bar{t}(1 - \bar{t})$) and σ_t^2 is variance of t (Wang et al., 2007).

Following Goel (1988), leaf inclination angle distributions can be described using six parametric ‘archetype’ functions based on empirical

Table 1

Statistical moments (i.e., number of observations, mean, standard deviation, two parameters μ, ν) of the leaf angle measurements and the LAD function type (after De Wit, 1965) from the LDP and TLS approaches for the simulated RAMI IV tree representations. PL – planophile, PG – plagiophile, U – uniform, S – spherical, E – erectophile.

Tree representation	LDP					TLS						
	n	Mean	S.D.	u	v	Type	n	Mean	S.D.	u	v	Type
ACPL	279	55.71	24.80	0.80	1.30	S	177342	61.42	21.11	0.93	2.01	E
ALGL3	183	48.66	23.55	1.21	1.42	U	164372	42.98	21.32	1.8	1.65	U
BEPE2	224	40.26	18.24	2.77	2.25	PG	73685	42.54	19.18	2.37	2.12	PG
FREX	152	31.21	21.49	1.94	1.03	PL	252275	33.62	23.18	1.58	0.94	PL
TICO2	116	40.83	17.84	2.90	2.41	PG	228446	46.67	18.9	2.24	2.42	PG

Table 2

Optimal parameter values for TLS LAD estimates, detected by sensitivity analysis using simulated data. MAE stands for Mean Absolute Error.

Distance (m)	kNN	Eigenvalue ratio threshold	MAE mean	MAE std
10	10	0.15	0.013	0.008
20	10	0.10	0.011	0.007
30	5	0.10	0.012	0.008
40	5	0.10	0.015	0.009
50	10	0.15	0.018	0.012

evidence of the natural variation of leaf normal distributions: spherical, uniform, planophile, plagiophile, erectophile and extremophile. For spherical canopies, the relative frequency of leaf inclination angles is the same as the relative frequency of the inclinations of the surface elements of a sphere; for uniform canopies, the proportion of leaf inclination angles is the same at any angle; planophile canopies are characterized by a predominance of horizontally oriented leaves; plagiophile canopies are dominated by inclined leaves, erectophile canopies are dominated by vertically oriented leaves, and extremophile canopies by high frequencies of both horizontally and vertically oriented leaves (Lemeur and Blad, 1974). As these classical distributions are widely used and easier to interpret than the parameter values of the Beta distribution, we classified all estimated leaf inclination angle distributions by finding the closest archetype distribution. For each measured distribution, the deviation from the distributions suggested by de Wit (f_{deWit}) was quantified using a modified version of the inclination index provided by Ross (1975):

$$\chi_L = \int_0^{\pi/2} |f(\theta_L) - f_{deWit}(\theta_L)| d\theta_L \tag{7}$$

3. Results and discussion

3.1. LAD retrieval from TLS and LDP: simulated tree representations

It should be noted that the simulated leaves had no curvature, which removed one source of uncertainty for estimating the leaf angles with the LDP measurement technique in particular. Overall, the agreement between TLS- and LDP-based measurement techniques using the 3D tree simulations was with R squares between 0.45 (ALGL3; Fig. 10B) and 0.8 (ACPL, Fig. 10A) for actual measurements. Importantly, the simulated trees covered the full range of possible leaf angle probability density functions (PDFs), and both approaches agreed on the assigned de Wit type (1965), except the ACPL tree representation (LDP – spherical; TLS – erectophile) (Table 1). Even in this case the difference in the mean values between the two approaches was less than 6°, which is within the limits of the previously identified uncertainty of the LDP measuring technique by Raabe et al. (2015). The TLS-based PDFs agreed to within 84% with the prescribed leaf element frequencies of the RAMI-IV trees (Fig. 10). The agreement between the prescribed and retrieved PDFs was linked to the foliage density. The ALGL3 and BEPE2 RAMI-IV trees had very dense foliage, which can obscure and make it more

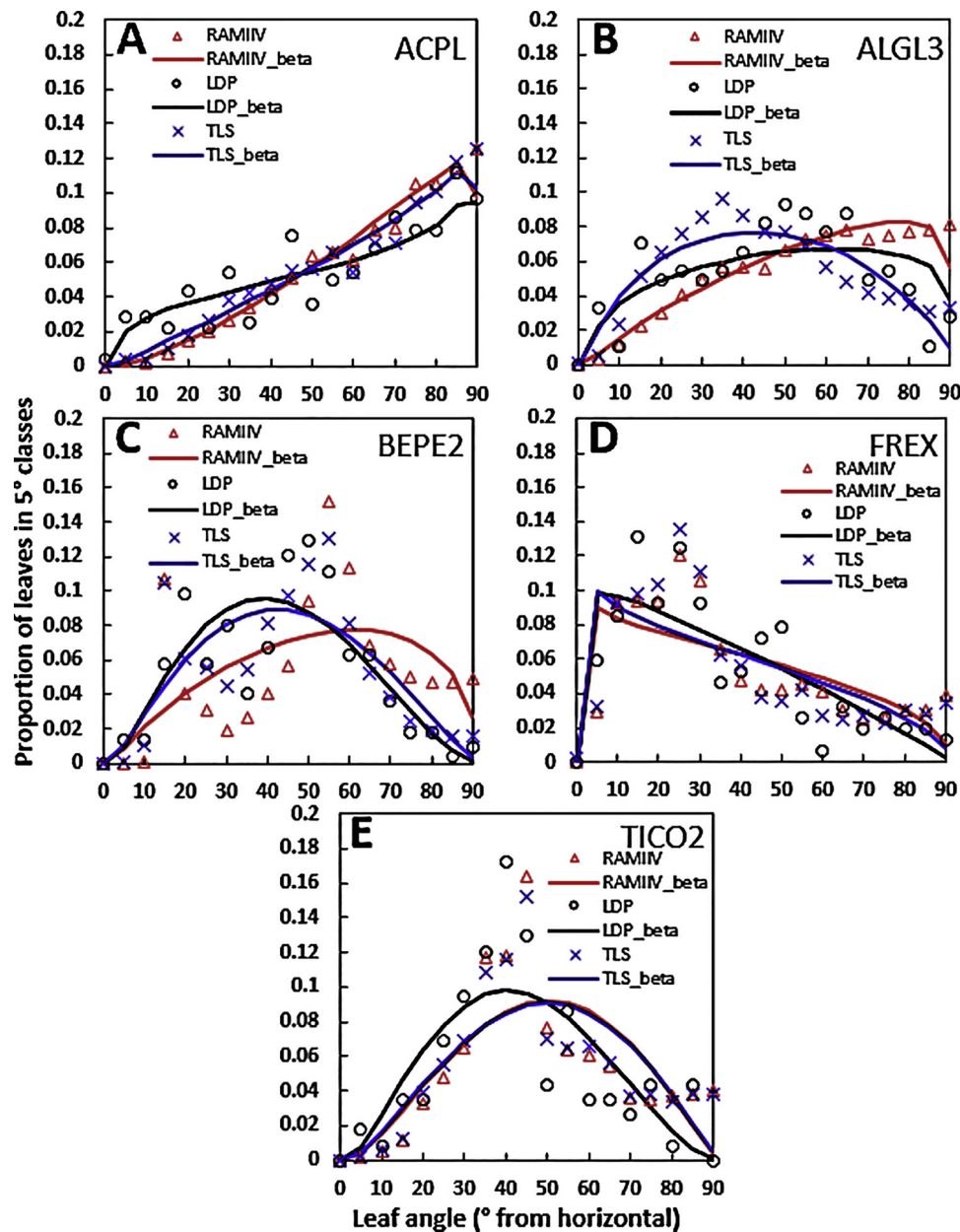


Fig. 10. Frequency and fitted beta distributions of leaf angle for the simulated tree representations for RAM-IV Järvselja birch stand. Differences in the distributions between LDP (black), TLS (blue) and RAMI IV (red) representations as tested by Chi-square two sample test were non-significant at $p < 0.05$ for all measured species (For interpretation of the references to colour in this figure legend, the reader is referred to the web version of this article).

challenging to sample leaves located deeper within the tree crowns. The dense foliage of these trees, and the way individual leaves were represented in the simulated images with sometimes not so distinct outlines (see Fig. 1B for an example), posed additional challenges to identifying suitable leaves and sample the whole crown space evenly with the LDP measurement approach. This was mainly due to the decreased contrast between the potential target and background (Fig. 1B). Still, both TLS and LDP measurement techniques were able to provide PDFs that correctly approximated even the bi-modal PDF prescribed for the BEPE2 tree simulation (Fig. 10C). Fig. 10 also illustrates the agreement between the PDFs and the fitted beta distributions. This shows similar results to Wang et al. (2007), who evaluated the two-parameter beta distribution as the more consistent and robust predictor over other approaches.

Fig. 11 demonstrates the effect of TLS distance on the LAD information retrieval. There is a tendency towards more vertical PDF

retrieval by TLS with an increasing distance of the sensor from the target. If the LAD of a given target can be described as spherical or erectophile, then our simulation results indicate that TLS can provide good quality information even at a distance of 50 m (Fig. 11A). However, the results get progressively worse with distance if the ‘true’ LAD can be described as rather horizontally oriented (Fig. 11B–E). For the planophile case (FREX; Fig. 11E), the TLS-derived LAD type shifts to a different one (uniform) already at the distance of 20 m. We found that leaf size/area plays an important role in this change of LAD along different scanning distances. In fact, there is a linear relationship ($R^2 = 0.99$) between individual leaf areas, provided in the reference data for each tree model (Widłowski et al., 2015), and the variation of each tree’s LAD over distance. In this case MAE is inversely proportional to leaf area, which means that LAD estimates from small leaves will have a larger degradation of accuracy over scanning distance.

Variations in scanning distance also affect the capability of a LiDAR

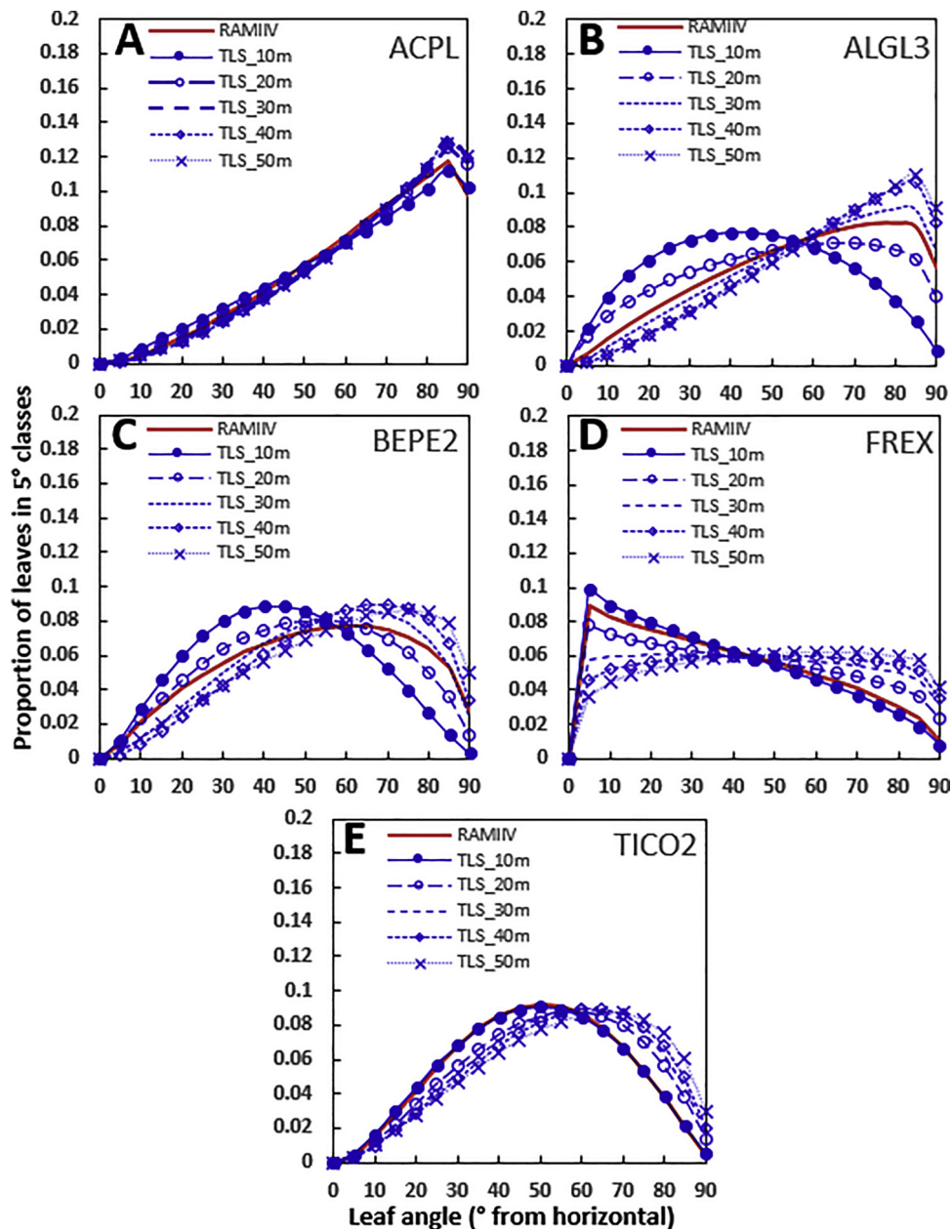


Fig. 11. Effect of varying TLS-target distance on the LAD retrieval from TLS for the select RAMI IV tree representations.

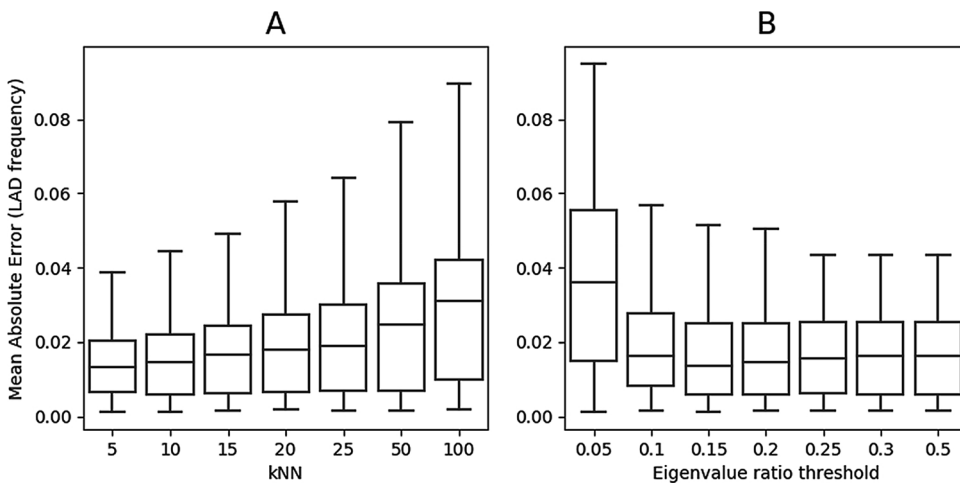


Fig. 12. Box whisker showing Mean Absolute Error (MAE) of TLS LAD estimates method over a range of kNN and eigenvalues ratio threshold. Results were aggregated from all simulated point clouds used in the validation of our TLS method. The box dimensions show the quartiles for 25% to 75% of MAE, the center line represents median MAE and the whiskers show minimum and maximum MAE.

scanner to detect and resolve leaves of different inclination angles. Using a hypothetical leaf at 10 m from the ground, a laser beam will have an inclination angle of 45° at 10 m from the tree and an angle of 11.3° at 50 m from the tree. This means that leaves with a low inclination angle, i.e. horizontal leaves, will have a considerably smaller projected area on the laser sensor. Also, as the scanning angle resolution was the same for all simulations, the point density (number of points per unit of area) scaled down based on the area of a scanned hemisphere. So in the case of our simulated point clouds, the point density was reduced by an average of 86% ($\pm 8\%$) when changing scanning distances from 10 m to 50 m. The combination of these factors means that with increasing distance from the tree, leaves with lower inclination angles will be less likely to be intersected by a laser beam, which helps to explain why there is a shift towards erectophile LADs for longer scanning distances. The lower individual leaf area for ALGL3 and BEPE2 is contributing factor that makes this effect even more pronounced for these trees.

3.2. Sensitivity analysis of LAD retrieval from TLS

We used the simulated point clouds to perform a sensitivity analysis of our TLS method over a range of kNN and eigenvalues ratio threshold. Results of the sensitivity tests (Fig. 12) show that our TLS method is able to estimate LAD with an average MAE of 0.018 (standard deviation of 0.012). Fig. 12 also helps to understand how changes in each parameter impact the accuracy in LAD estimates. The results suggest that lower values for kNN, e.g. 5 or 10, and filtering thresholds of above 0.1 are optimal. However, we note that the assessment of the impact of threshold values (Fig. 12b) might have been limited due to the lack of noise and overlapping leaves in our simulated data. A set of optimal parameters values was also generated for each scanning distance (Table 2) and a comparison of LAD estimates using these parameters against the RAMI-IV reference data is shown in Fig. 13.

The curvature analysis showed that the TLS method is able to predict LAD from curved leaves with MAE lower than 0.11 for all cases (Fig. 14). The curvature validation suggests that our TLS method is able to accurately predict LAD from curved leaves and that point density is a major constraining factor in the accuracy of LAD estimates. For a comparison, the point density of a single scan using an angular step resolution of 0.04° is around 20,000 points/m² at 10 m and 1000 points/m² at 50 m. Fig. 8 shows that even for a hypothetical completely curved leaf point cloud, with point density relative to a 50 m single scan, the MAE of a TLS LAD is still lower than 0.11. In tests with higher point densities the MAE lowers to below 0.04. Also, for a completely flat leaf the MAE is lower than 0.001 overall. However, we note that

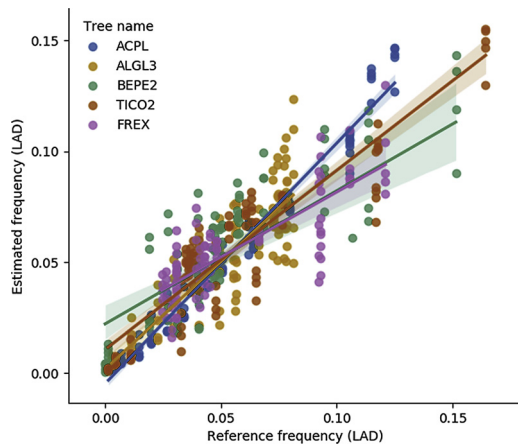


Fig. 13. 1:1 simulated trees TLS LAD comparison grouped by tree. Solid lines represent linear regression fitted to each tree's LAD comparison scatter points. Shaded areas represent a confidence interval of 95% for each regression.

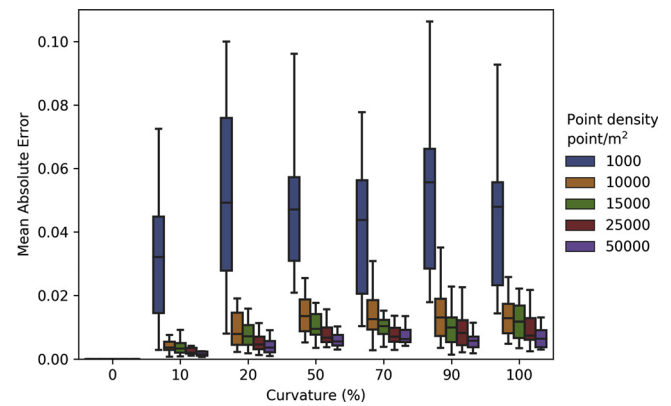


Fig. 14. Box whisker showing Mean Absolute Error (MAE) of TLS LAD estimates method for different leaf curvatures and point densities. Results were aggregated for all hypothetical leaves used in the curvature tests. The box dimensions show the quartiles for 25%–75% of MAE, the center line represents median MAE and the whiskers show minimum and maximum MAE.

this was an hypothetical point cloud with no noise, occlusion or overlapping leaves. In actual point clouds the MAE is expected to be higher, especially for leaves scanned from longer distances (e.g. > 30 m). The impact of point density also suggests that the use of multiple scans should improve the accuracy of LAD estimates.

3.3. LAD retrieval from TLS and LDP: real trees

Next, we compared LDP and TLS measurement techniques using real trees. Similarly, to the model tree representations described above, the pool of sampled real trees at Kew contained a wide range of LAD types, from broadly plagiophile (*Diospyros lotus*) to erectophile (*Ostrya japonica*) case. Results show that very similar results (fitted Beta distributions) can be obtained using different LDP measurement techniques (images taken with a digital camera mounted on a tripod or a hand-balanced smart phone; Fig. 15). Compared to tripod-based camera approach, smart phone based acquisition provides up to ten times faster and more flexible approach, and it is encouraging these advantages are not offset by the accuracy of the method, if a large enough sample pool is collected (Table 3).

Results show that the agreement between TLS and LDP measurement techniques were lower than those obtained from the simulated tree representations. Compared to the simulated cases, the sampled trees at Kew possessed leaves with various curvatures, and the effect of leaf curvature was clearly captured in the agreements between TLS and LDP measurement techniques for given species. The agreement between the fitted Beta distributions for the TLS and LDP approaches for *Wollemia nobilis* (Fig. 15) was 97%. *Wollemia nobilis* possesses relatively short leaves with no transverse curvature. The sampled *Diospyros lotus* tree had leaves with various curvature rates, and the bent leaves of *Ginkgo biloba* were the most challenging for applying the LDP measurement technique, which relies on identifying rather flat leaves oriented approximately perpendicular to the viewing direction of the digital camera/lens. This challenge was subsequently reflected in the greater difference between both retrieved PDFs and fitted Beta distributions for *Diospyros lotus* and *Ginkgo biloba*, compared to *Wollemia nobilis* (Fig. 15). However, it is notable that the LDP and TLS measurement techniques agreed in the assigned de Wit type in all cases bar one (Table 3). The only exception was *Ginkgo Biloba*, where LDP assigned spherical and TLS assigned erectophile LAD type. This was similar to the ACPL case from the simulated trees described above in Section 3.1. It should be noted that the resulting leaf projection or G function (Ross, 1981), which describes the projection of unit foliage area on the plane perpendicular to the view direction (Myneni et al., 1989; Ross, 1981), is rather similar between spherical and erectophile

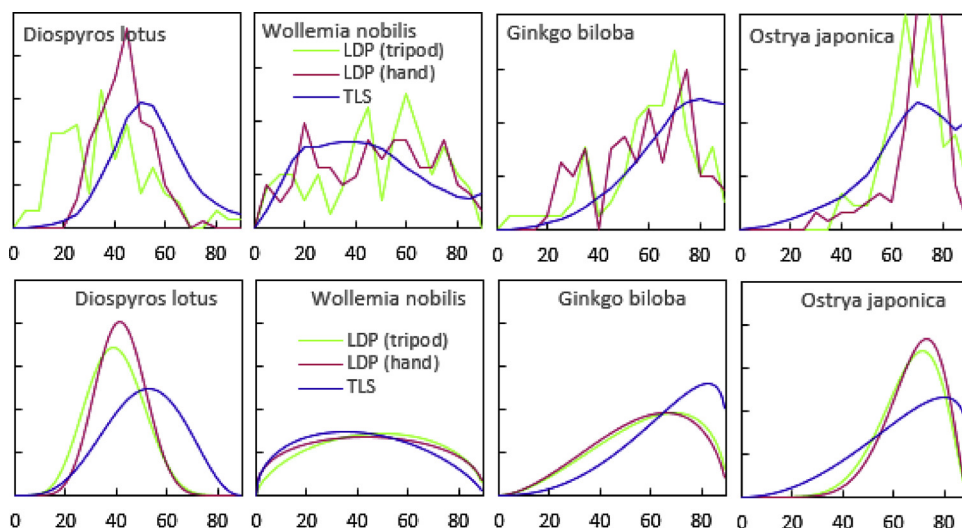


Fig. 15. Frequency (top) and fitted beta distributions (bottom) of leaf angle for the four tree species at Kew, measured from the tripod-stabilized leveled digital photography (LDPT – green line), hand-balanced digital photography (LDPh – pink line) and terrestrial laser scanner (TLS – blue line) (For interpretation of the references to colour in this figure legend, the reader is referred to the web version of this article).

canopies (Ryu et al., 2010; Pisek et al., 2013).

3.4. Implications for the future potential of TLS to retrieve LAD information

Our results are very encouraging with respect to using our proposed TLS measurement technique for the retrieval of LAD information. At the same we also discuss the potential limits of the method. The validation of previously proposed methods to retrieve LAD information with TLS data (e.g. Zheng and Moskal, 2012; Jin et al., 2015; Bailey and Mahaffee, 2017) was done with smaller, isolated trees or shrubs with TLS positioned at a close distance to targets. Here, for the first time we demonstrate the possible limitation of TLS measurement techniques for the retrieval of LAD information for more distant canopies, or for taller trees ($h > 20$ m).

Compared to the LDP measurement technique, TLS is not limited by leaf curvature, and depending on the distance might be even capable of retrieving leaf angle information from more complex leaf surfaces. Consequently, TLS might provide more accurate information about LAD than LDP in these cases, albeit the assigned de Wit may well still be the same for LDP and TLS (Table 1). TLS might be also applicable in cases where LDP is not an option (severely bent, twisted leaves). This way TLS measurements might allow us to extend greatly the pool of plant species for which we could retrieve LAD information, particularly for taller trees, which is so crucial for correct RT modelling in vegetation canopies (Govind et al., 2013). It remains to be seen if TLS can provide us with good quality information about needleleaf canopies as well. Our TLS method can also provide further information about leaf angles, such as 3D partitioning of the leaf points, which could assist on further insights into how leaf angle changes over height or different directions (Fig. 8E). An example of inclination and azimuth angles partitioning across crown height is shown in Fig. 16, which shows not only how leaf angles vary for different partitions but also how much each partition

represents in the total amount of leaf material. We note that azimuth angles estimates are not within the scope of this paper and such information is just provided as an example of possible outcomes of our TLS leaf angle method. One final issue to consider is that currently, TLS instruments are in general much more expensive than cameras, and their operation characteristics are also more variable e.g. time-of-flight v phase shift, beam divergence, angular resolution etc. Consequently, the point clouds from different sensors and acquisitions will have varying potential for LAD retrieval. These aspects will need to be explored further in order to allow better understanding of the resulting uncertainties, and to allow direct comparison between different studies.

4. Conclusions

In this study we introduce a fast and simple method for detection of LAD information from terrestrial LiDAR scanning (TLS) point clouds. Our findings provide support for the following conclusions:

- 1) LAD information can be obtained by simply accumulating all valid planes fitted to points in a leaf point cloud.
- 2) Compared to the LDP measurement technique, TLS is not limited by leaf curvature, and depending on the distance of the scanner (i.e. the footprint of the TLS at the target), might be even capable of retrieving leaf angle information from more complex leaf surfaces.
- 3) TLS measurement techniques might be limited for the retrieval of accurate LAD information for more distant canopies, or for taller trees ($h > 20$ m). We recommend keeping the scanning distance within 20 m from the target canopy and the use of multiple (> 2) scans from different positions around the trees to improve leaf detection.

Table 3

Statistical moments (i.e., number of observations, mean, standard deviation, two parameters μ , ν) of the leaf angle measurements and the LAD function type (T), after De Wit (1965) from the tripod-stabilized leveled digital photography (LDPT), hand-balanced digital photography (LDPh) and terrestrial laser scanner (TLS) approaches at the Kew Royal Botanical Gardens. PG – plagiophile, U – uniform, S – spherical, E – erectophile. ID represents the tree identifier: DL - *Diospyros lotus*, GB - *Ginkgo biloba*, OJ - *Ostrya japonica*, WN - *Wollemia nobilis*.

ID	LDPT						LDPh						TLS					
	n	Mean	S.D.	μ	ν	T	n	Mean	S.D.	μ	ν	T	n	Mean	S.D.	μ	ν	T
DL	100	39.59	11.00	8.68	6.82	PG	120	41.67	9.52	11.39	9.82	PG	212595	50.85	14.64	3.6	4.68	PG
GB	78	57.67	18.90	1.52	2.70	S	80	56.28	18.78	1.64	2.74	S	277167	65.92	16.95	1.21	3.31	E
OJ	90	66.37	11.63	2.78	7.81	E	120	68.09	10.92	2.80	8.70	E	165189	63.68	17.79	1.26	3.04	E
WN	80	46.71	22.05	1.52	1.64	U	123	44.44	23.06	1.42	1.39	U	205368	41.25	21.82	1.75	1.48	U

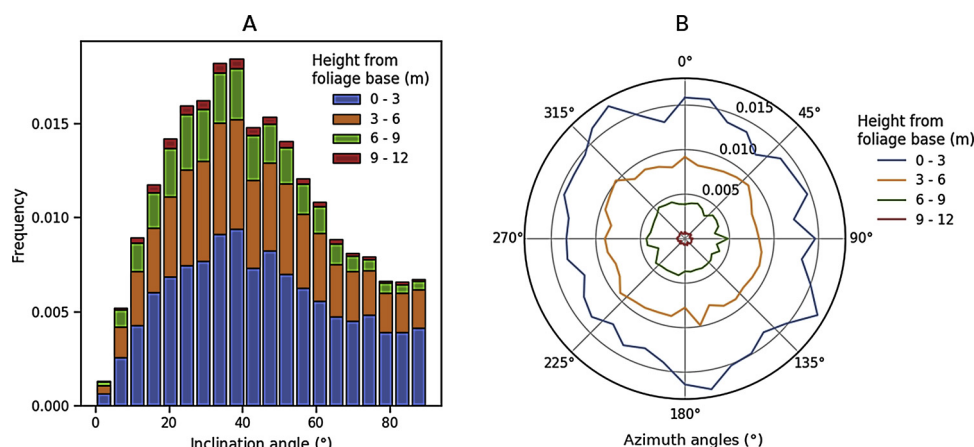


Fig. 16. Zenith (A) and azimuth (B) leaf angle distributions over 3 m vertical slices along the crown height estimated from ALGL3 point clouds at 10 m scanning distance.

Acknowledgments

JP was supported by the Estonian Research Council grant PUT1355 and Mobilitas PlussMOBERC-11. MBV was supported by the Science Without Borders grant 233849/2014-9 from the National Council of Technological and Scientific Development – Brazil. MD acknowledges the support of the NERC National Centre for Earth Observation for the provision of TLS equipment. MD was also supported in part by NERC Standard Grants NE/N00373X/1 and NE/P011780/1, and European Union's Horizon 2020 research and innovation programme under grant agreement No 640176 for the EU H2020 BACI project.

We gratefully acknowledge the invaluable help of staff at Kew Gardens, in particular: Amanda Cooper, Tony Kirkham and Justin Moat. We thank Dr. Youngryel Ryu and another anonymous reviewer for constructive comments.

References

- Asner, G.P., 1998. Biophysical and biochemical sources of variability in canopy reflectance. *Remote Sens. Environ.* 64, 234–253.
- Bailey, B.N., Mahaffee, W.F., 2017. Rapid measurement of the three-dimensional distribution of leaf orientation and the leaf angle probability density function using terrestrial LiDAR scanning. *Remote Sens. Environ.* 193, 63–76.
- Bauwens, S., Bartholomeus, H., Calders, K., Lejeune, P., 2016. Forest inventory with terrestrial LiDAR: comparison of static and hand-held mobile laser scanning. *Forests* 7, 127.
- Calders, K., Lewis, P., Disney, M., Verbesselt, J., Herold, M., 2013. Investigating assumptions of crown archetypes for modelling LiDAR returns. *Remote Sens. Environ.* 134, 39–49.
- Calders, K., Newnham, G., Burt, A., Murphy, S., Raunonen, P., Herold, M., Culvenor, D., Avitabile, V., Disney, M., Armston, J., Kaasalainen, M., 2015. Nondestructive estimates of above-ground biomass using terrestrial laser scanning. *Methods Ecol. Evol.* 6, 198–208.
- Côté, J.-F., Fournier, R.A., Frazer, G.W., Niemann, K.O., 2012. A fine-scale architectural model of trees to enhance LiDAR-derived measurements of forest canopy structure. *Agric. For. Meteorol.* 166, 72–85.
- De Wit, C.T., 1965. Photosynthesis of Leaf Canopies. Agricultural Research Report No. 663, Wageningen. <http://library.wur.nl/WebQuery/wurpubs/413358>.
- Disney, M., Lewis, P., Saich, P., 2006. 3D modelling of forest canopy structure for remote sensing simulations in the optical and microwave domains. *Remote Sens. Environ.* 100, 114–132.
- Disney, M.I., Lewis, P., Bouvet, M., Prieto-Blanco, A., Hancock, S., 2009. Quantifying surface reflectivity for spaceborne lidar via two independent methods. *IEEE Trans. Geosci. Remote Sens.* 47 (10), 3262–3271. <https://doi.org/10.1109/TGRS.2009.2019268>.
- Disney, M.I., Kalogirou, V., Lewis, P.E., Prieto-Blanco, A., Hancock, S., Pfeifer, M., 2010. Simulating the impact of discrete-return lidar system and survey characteristics over 2 young conifer and broadleaf forests. *Remote Sens. Environ.* 114, 1546–1560. <https://doi.org/10.1016/j.rse.2010.02.009>.
- Disney, M.I., Lewis, P., Gomez-Dans, J., Roy, D., Wooster, M., Lajas, D., 2011. 3D radiative transfer modelling of fire impacts on a two-layer savanna system. *Rem. Sens. Environ.* 115, 1866–1881. <https://doi.org/10.1016/j.rse.2011.03.010>.
- Disney, M.I., Boni Vicari, M., Calders, K., Burt, A., Lewis, S., Raunonen, P., Wilkes, P., 2018. Weighing Trees With Lasers: Advances, Challenges and Opportunities, Royal Society Interface Focus. special Issue on Royal Society meeting "The terrestrial laser scanning revolution in forest ecology" <https://doi.org/10.1098/rsfs.2017.0048>.
- Falster, D.S., Westoby, M., 2003. Leaf size and angle vary widely across species: what consequences for light interception? *New Phytol.* 158, 509–525.
- Goel, N.S., Strelbe, D.E., 1984. Simple beta distribution representation of leaf orientation in vegetation canopies. *Agron. J.* 76, 800–802.
- Goel, N.S., 1988. Models of vegetation canopy reflectance and their use in estimation of biophysical parameters from reflectance data. *Remote Sens. Rev.* 4, 1–213.
- Govind, A., Guyon, D., Roujean, J.-L., Yauschew-Raguens, N., Kumari, J., Pisek, P., Wigneron, J.-P., 2013. Effects of canopy architectural parameterizations on the modeling of radiative transfer mechanism. *Ecol. Modell.* 251, 114–126.
- Hackenberg, J., Morhart, C., Sheppard, J., Spiecker, H., Disney, M.I., 2014a. Highly accurate tree models derived from terrestrial laser scan data: a method description. *Forests* 5, 1069–1105.
- Hackenberg, J., Morhart, C., Sheppard, J., Spiecker, H., Disney, M.I., 2014b. Highly accurate tree models derived from terrestrial laser scan data - a method description, *Forests* (OPEN ACCESS). Special Issue: LiDAR and Other Remote Sensing Applications in Mapping and Monitoring of Forests Structure and Biomass) 5, 1069–1105. <https://doi.org/10.3390/f5051069>.
- Hosoi, F., Omasa, K., 2007. Factors contributing to accuracy in the estimation of the woody canopy leaf area density profile using 3D portable lidar imaging. *J. Exp. Bot.* 58 (12), 3463–3473.
- Jin, S., Tamura, M., Susaki, J., 2015. A new approach to retrieve leaf normal distribution using terrestrial laser scanners. *J. For. Res.* 27, 631–638.
- Király, G., Broly, G., 2007. Tree Height Estimation Methods for Terrestrial Laser Scanning in a Forest Reserve. Proceedings of ISPRS Workshop on laser scanning 2007 and SilviLaser, Espoo, Finland, pp. 211–215 12-14 September, 2007.
- Klasing, K., 2009. Surface-based Segmentation of 3D Range Data. Technical Report TR-LSE-2009-10-1. Institute of Automatic Control Engineering, Technische Universität München, Germany.
- Kucharik, C., Norman, J.M., Gower, S.T., 1998. Measurements of leaf orientation, light distribution and sunlit leaf area in a boreal aspen forest. *Agric. Forest Meteorol.* 91, 127–148.
- Kuusik, A., Lang, M., Kuusik, J., 2013. Database of optical and structural data for the validation of forest radiative transfer models. In: In: Kokhanovsky, A. (Ed.), *Light Scattering Reviews*, vol. 7. Springer, Berlin, Heidelberg, pp. 109–148.
- Lang, A.R.G., 1973. Leaf orientation of a cotton plant. *Agric. For. Meteorol.* 11, 37–51.
- Lemeur, R., Blad, B.L., 1974. A critical review of light models for estimating the short-wave radiation regime of plant canopies. *Agric. For. Meteorol.* 14, 255–286.
- Lewis, P., 1999. Three-dimensional plant modelling for remote sensing simulation studies using the Botanical Plant Modelling System. *Agron. Agric. Environ.* 19, 185–210.
- Malhi, Y., Bentley, L.P., Jackson, T., Lau, A., Shenkin, A., Herold, M., Calders, K., Bartholomeus, H., Disney, M.I., 2018. Understanding the Ecology of Tree Structure and Tree Communities Through Terrestrial Laser Scanning. Royal Society Interface Focus, special Issue on Royal Society meeting "The terrestrial laser scanning revolution in forest ecology" <https://doi.org/10.1098/rsfs.2017.0052>.
- Mandel, J., 1982. Use of the singular value decomposition in regression analysis. *Am. Stat.* 36 (1), 15–24. <https://doi.org/10.2307/2684086>.
- McNeil, B.E., Pisek, J., Lepik, H., Flamenco, 2016. E. A. Measuring leaf angle distribution in broadleaf canopies using UAVs. *Agric. For. Meteorol.* 218–219, 204–208. <https://doi.org/10.1016/j.agrformet.2015.12.058>.
- Müller-Linow, M., Pinto-Espinosa, F., Scharr, H., Rascher, U., 2015. The leaf angle distribution of natural plant populations: assessing the canopy with a novel software tool. *Plant Methods* 11, 1–16.
- Myneni, R.B., Ross, J., Asrar, G., 1989. A review on the theory of photon transport in leaf canopies. *Agric. For. Meteorol.* 45, 1–153.
- Ollinger, S.V., 2011. Sources of variability in canopy reflectance and the convergent properties of plants. *New Phytol.* 189, 375–394.
- Origo, N., Calders, K., Nightingale, J., Disney, M.I., 2017. Influence of levelling technique on the retrieval of canopy structural parameters from digital hemispherical photography. *Agric. For. Meteorol.* 237–238, 143–149. <https://doi.org/10.1016/j>

- agrformet.2017.02.004.
- Palace, M., Sullivan, F.B., Ducey, M., Herrick, C., 2016. Estimating tropical forest structure using a terrestrial lidar. *PLoS One* 11 (4). <https://doi.org/10.1371/journal.pone.0154115>. e0154115.
- Pfennigbauer, M., Ullrich, A., 2010. Improving quality of laser scanning data acquisition through calibrated amplitude and pulse deviation measurement. In: In: Turner, M.D., Kamerman, G.W. (Eds.), *PIE 7684, Laser Radar Technology and Applications XV*, vol. 7684 pp. 76841F.
- Pisek, J., Ryu, Y., Alikas, K., 2011. Estimating leaf inclination and G-function from leveled digital camera photography in broadleaf canopies. *Trees* 25, 919–924.
- Pisek, J., Sonnentag, O., Richardson, A.D., Möttus, M., 2013. Is the spherical leaf inclination angle distribution a valid assumption for temperate and boreal broadleaf tree species? *Agric. For. Meteorol.* 169, 186–194.
- Prasad, O.P., Hussinb, Y.A., Weirb, M., Karnac, J.C., Yogendra, K., 2016. Derivation of forest inventory parameters for carbon estimation using terrestrial LIDAR. The International Archives of the Photogrammetry. *Remote Sens. Spatial Inf. Sci.* 677–684 XLI-B8.
- Raabe, K., Pisek, J., Sonnentag, O., Annuk, K., 2015. Variations of leaf inclination angle distribution with height over the growing season and light exposure for eight broadleaf tree species. *Agric. For. Meteorol.* 2–11 214–215.
- Raumonen, P., Kaasalainen, M., Akerblom, M., Kaasalainen, S., Kaartinen, H., Vastaranta, M., Holopainen, M., Disney, M., Lewis, P., 2013. Fast automatic precision tree models from terrestrial laser scanner data. *Remote Sens. (Basel)* 5, 491–520.
- Ross, J., 1975. Radiative transfer in plant communities. In: In: Monteith, J.L. (Ed.), *Vegetation and the Atmosphere*, vol. 1. Academic Press, London, UK, pp. 13–55.
- Ross, J., 1981. *The Radiation Regime and Architecture of Plant Stands*. Junk Publishers, The Hague, pp. 391.
- Ryu, Y., Sonnentag, O., Nilson, T., Vargas, R., Kobayashi, H., Wenk, R., Baldocchi, D.D., 2010. How to quantify tree leaf area index in a heterogeneous savanna ecosystem: a multi-instrument and multi-model approach. *Agric. For. Meteorol.* 150, 63–76.
- Smith, J.A., Berry, J.K., 1979. Optical diffraction analysis for estimating foliage angle distribution in grassland canopies. *Aust. J. Bot.* 27, 123–133.
- Stuckens, J., Somers, B., Delalieux, S., Verstraeten, W.W., Coppin, P., 2009. The impact of common assumptions on canopy radiative transfer simulations: A casestudy in citrus orchards. *J. Quant. Spectrosc. Radiat. Transf.* 110, 1–21. <https://doi.org/10.1016/j.jqsrt.2008.09.001>.
- Tadrist, L., Saudreau, M., de Langre, E., 2014. Wind and gravity mechanical effects on leaf inclination angles. *J. Theor. Biol.* 341, 9–16.
- Tanago, G.J., Lau, A., Bartholomeus, H., Herold, M., Avitabile, V., Raumonen, P., Martius, C., Goodman, R.C., Disney, M., Manuri, S., Burt, A., Calders, K., 2018. Estimation of above-ground biomass of large tropical trees with terrestrial LiDAR. *Methods Ecol. Evol.* 9, 223–234. <https://doi.org/10.1111/2041-210X.12904>.
- Vicari, M. (2017) *TLSeparation*. <http://doi.org/10.5281/zenodo.1147706>.
- Wang, W.M., Li, Z.I., Su, H.B., 2007. Comparison of leaf angle distribution functions: effects on extinction coefficient and fraction of sunlit foliage. *Agric. For. Meteorol.* 143, 106–122.
- Warren Wilson, J., 1959. Analysis of the spatial distribution of foliage by two dimensional point quadrats. *New Phytol.* 58, 92–99.
- Widłowski, J.-L., Robustelli, M., Disney, M.I., Gastellu-Etchegorry, J.-P., Laverigne, T., Lewis, P., North, P.R.J., Pinty, B., Thompson, R., Verstraete, M.M., 2008. The RAMI Online Model Checker (ROMC): a web-based benchmarking facility for canopy reflectance models. *accepted Rem. Sens. Environ.* 112 (3), 1144–1150. <https://doi.org/10.1016/j.rse.2007.07.016>.
- Widłowski, J.L., Mio, C., Disney, M., Adams, J., Andredakis, I., Atzberger, C., Brennan, J., Busetto, L., Chelle, M., Ceccherini, G., Colombo, R., Côté, J.F., Eenmäe, A., Essery, R., Gastellu-Etchegorry, J.P., Gobron, N., Grau, E., Haverd, V., Homolová, L., Huang, H., Hunt, L., Kobayashi, H., Koetz, B., Kuusk, A., Kuusk, J., Lang, M., Lewis, P.E., Lovell, J., Malenovsky, Z., Meroni, M., Morsdorf, F., Möttus, M., Ni-Meister, W., Pinty, B., Rautiainen, M., Schlerf, M., Somers, B., Stuckens, J., Verstraete, M.M., Yang, W., Zhao, F., Zenone, T., 2015. The fourth phase of the radiative transfer model inter-comparison (RAMI) exercise. Actual canopy scenarios and conformity testing. *Remote Sens. Environ.* 169, 418–437.
- Woodgate, W., Armston, J., Disney, M.I., Suarez, L., Jones, S.D., Hill, J., Wilkes, P., Soto-Berelov, M., 2016. Quantifying the impact of woody material on leaf area index estimation from hemispherical photography using 3D canopy simulations. *Agric. For. Meteorol.* 226–227, 1–12. <https://doi.org/10.1016/j.agrformet.2016.05.009>.
- Zheng, G., Moskal, L.M., 2012. Leaf orientation retrieval from terrestrial laser scanning (TLS) data. *IEEE Trans. Geosci. Remote Sens.* 50, 3970–3979.
- Zhao, K., et al., 2015. Terrestrial lidar remote sensing of forests: maximum likelihood estimates of canopy profile, leaf area index, and leaf angle distribution. *Agric. For. Meteorol.* 209–210, 100–113.
- Zou, X., Möttus, M., Tammeorg, P., Torres, C.L., Takala, T., Pisek, J., Mäkelä, P., Stoddard, F.L., Pellikka, P., 2014. Photographic measurement of leaf angles in field crops. *Agric. For. Meteorol.* 184, 137–146.